Mechanics of twisted hippuric acid crystals untwisting as they grow

5 AUTHORS, INCLUDING:

Xiaoyan Cui
New York University

8 PUBLICATIONS **273** CITATIONS

SEE PROFILE

Bart Kahr
New York University

215 PUBLICATIONS **2,981** CITATIONS

SEE PROFILE

Mechanics of twisted hippuric acid crystals untwisting as they grow†

Alexander G. Shtukenberg,*[a] Ankit Gujral,[a] Elena Rosseeva,[b] Xiaoyan Cui[a] and Bart Kahr*[a]

Spontaneous twisting of single crystals is a common growth induced deformation. But as twisted crystals thicken they can untwist, restoring a straight form. The mechanics of this process was studied for vapor grown needle-like crystals of *N*-benzoylglycine (hippuric acid) and *N*-(2-thienylcarbonyl)glycine, and analyzed by phenomenological models. The elastic stress at the crystal tip undergoes plastic relaxation leading to the twisting deformations. As the crystal grows and thickens it partially untwists showing linear increases of the twist period with crystal thickness. Such behavior was simulated with a model that assumes the constant density of defects in successive growth layers. However, transmission electron microscopy does not reveal any dislocations or other extended defects typically associated with plastic deformation. Published data on other materials show the linear dependencies of pitch on thickness suggesting comparable untwisting mechanisms for different materials.

Introduction

It is well established that growing crystals can undergo spontaneous mechanical transformations even in the absence of phase transformations or ostensible chemical change. Frequently, such transformations result in crystals with bent, twisted, and scrolled morphologies, among the variety of complex, non-polyhedral shapes observed. Such growth-actuated deformations are manifest in many types of materials and occur under variety of growth conditions.[1] For most such crystalline objects, the mechanisms of deformation remain a mystery. Establishing these mechanisms is an active area of investigation.

Twisting is by far the most common type of growth-induced deformation observed in the crystal kingdom. Many twisted crystals will untwist as they continue to grow. As twisting and untwisting are reciprocal processes, a focus on the mechanisms of untwisting will surely shed some light on those processes associated with growth induced twisting. In this report, we emphasize growing crystals that seemingly, spontaneously, untwist themselves.

Previously proposed mechanisms of twisting can be divided into three groups: (1) defects that form *via* specific crystal growth mechanisms and mediate deformation; (2) temperature, electrical, mechanical, and/or concentration fields that create a mechanical force acting on a growing crystal; (3) internal compositional and structural inhomogeneities that lead to lattice mismatch with the creation of a mechanical moment at the growth front.[1] Although all three processes may be operative under some conditions, the third seems to be the most common and universal.

Here, we focus on mechanical aspects of twisting deformations for a common class of crystalline objects, thin, extended crystals twisted around their elongation direction. We do not solve corresponding viscoelastic problems explicitly, but use a simplified approach to analyze possible scenarios depending on the distribution of the driving force for twisting over the crystal volume, the growth history, and the mechanical properties of the material.

It is known that twisting is influenced by cross-sectional size. A great deal of experimental data are plotted in Fig. 20 of ref. 1. Unfortunately, analysis of this data is complicated because aspects ratios are themselves dependent on growth conditions. In Fig. 1 we plot only the data obtained for single crystals growing under similar conditions. We also do not include data for crystals whose twisting is induced by axial screw dislocations (Eshelby twist)[2] because such crystals are well known to conform to the proportionality $P \sim h^2$,[3] where P is the twist period (pitch or a crystal length corresponding to π rotation) and h is the minimum cross sectional size. Fitting with a power function $P = kh^n$ has revealed that in most cases $0.6 \leq n \leq 1.3$ (for oxalic acid dihydrate $n = 0.3$ and melt grown *N*-benzoylglycine (hippuric acid, HA) $n = 1.9$).

[a] *Molecular Design Institute and Department of Chemistry, 100 Washington Square East, Silver Center, Room 1001, New York University, New York, NY 10003, USA. E-mail: shtukenberg@mail.ru, bart.kahr@nyu.edu*
[b] *Department of Chemistry, Zukunftskolleg, University of Konstanz, Box 714, 78457 Konstanz, Germany*
† Electronic supplementary information (ESI) available. See DOI: 10.1039/c5ce00195a
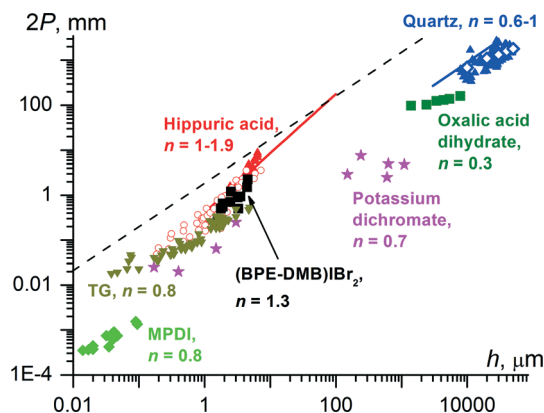
Fig. 1 Correlation between full twist period ($2P$, 2π rotation, mm) and the smallest crystal size in a cross section (h, μm). Blue symbols: quartz (up triangles,[6] open diamonds,[7] line (number of points, $N > 200$)[8]); Olive squares: oxalic acid dihydrate;[7] Magenta stars: potassium dichromate;[9,10] Black squares: (1,4-bis[2-(pyrene-1-yl) vinyl]-2,5-dimethylbenzene)IBr$_2$, (BPE-DMB)IBr$_2$;[11] Red symbols: hippuric acid (up triangles = melt grown crystals;[12] Open circles = vapor grown crystals; line = melt and solution grown crystals ($N = 60$)[13]; Dark yellow down triangles: N-(2-thienylcarbonyl)glycine, TG; Green diamonds: poly(m-phenylene isophthalamide), MPDI.[14] The values of n are exponents in the fit $P = kh^n$. In the region below the dashed line, $2P < 10^3\pi h$, elastic stress in twisted crystals should relax, at least partially.

Moreover, *all* data can be well fitted with a linear function, $P = k_0 + k_1 h$ (Fig. S1†). The presumption of a multistage growth mechanism, as from a seed, for example, obviates the complications of a non-zero coefficient k_0 that would lead to a nonsensical non-zero pitch for a vanishingly thin lamella. Thus, for all twisted crystals (excluding those twisted by the Eshelby mechanism) in the size range from nm to cm, twist period is proportional to the cross section size, $P \sim h$. This universal dependence promises insight into crystal twisting mechanisms and mechanics. Strain near the crystal surface, $\gamma = \pi h/(2P)$, typically exceeds 10^{-3} (Fig. 1). This value corresponds roughly to the upper limit of yield strain in most materials.[1,4,5] Deformation of all crystals in Fig. 1 is, at least partially, plastic, and the stress relaxation should be involved in any model of crystal deformation.

Here, we present detailed analysis of twisting in HA and N-(2-thienylcarbonyl)glycine (TG) crystals (Scheme 1). These compounds are isostructural and crystallize in the orthorhombic space group $P2_12_12_1$ with the lattice constants. $a = 9.112(2)$ Å, $b = 10.566(2)$ Å, $c = 8.855(2)$ Å[15] and $a = 9.467(2)$ Å, $b = 10.643(8)$ Å, $c = 8.653(6)$ Å,[16] respectively. The standard setting of the point group 222 is used. HA is known to easily
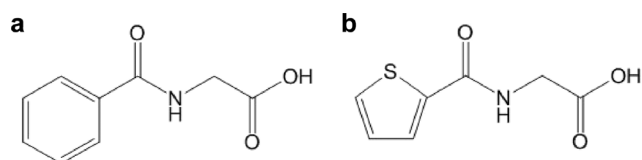
form twisted crystals from the melt and solutions.[12,13,17–19] Twisting occurs along [100] and [001] growth directions at $T = 60–175$ °C (melting point $T_m = 188$ °C). Twisting of TG crystals was not reported previously but our preliminary experiments have shown that twisted [100] elongated fibers form in spherulites growing from the melt at ~120 °C ($T_m = 167$ °C). The spherulite fibers twist only if melt is held near the melting point long enough to develop a violet decomposition product.

Experimental section

Materials and crystallization procedure

We used HA (98% Sigma-Aldrich) and TG synthesized in our laboratory.[16] Above the melting temperature HA becomes a dark wine red while the TG melt becomes violet. Melted HA was recrystallized from ethanol to yield pink crystals that were subsequently used for sublimation experiments. TG was used as synthesized.

HA and TG were crystallized by condensation from the vapor phase. A small amount (*ca.* 0.1 g) of each material was placed on the bottom of 20 mL glass vial. A piece of glass slide (*ca.* 40 × 12 mm) was placed diagonally inside the vial to serve as a substrate for crystallization. Then the vial was closed with its plastic cap and placed onto a Kofler bench at $T_{bench} = 100–220$ °C for 1 min – 45 days, with most crystals grown at $T_{bench} = 170–200$ °C for 3 min – 1 day. Since the temperature inside the vial differed from T_{bench}, an approximate calibration was developed from melting standards placed along the glass substrate (Fig. 2a). The growth rate changes fives orders of magnitude as T_{bench} increases from 100 to 215 °C (Fig. 2b).

Characterization

The glass substrate with crystals was cut in pieces and mounted on conductive carbon tape adhered to aluminum holders. Alternatively, crystals were detached from the glass substrate and then placed on the tape. The samples were coated with 5 nm gold or 4 nm iridium films and crystal morphologies were recorded with a MERLIN field-emission scanning electron microscope (SEM) (Carl Zeiss) using a standard Everhart–Thornley type detector at an acceleration voltage of 1–2.5 kV.

Crystals were indexed with an Olympus BX50 polarized light optical microscope using available data on the orientation of optical indicatrix in HA[12,20] and TG.[16] Height and deflection images of the crystal surface micromorphology were obtained with an atomic force microscope (AFM) (MFP-3D-SA System, Asylum Research) working in contact mode at a deflection of −2.0 V.

In order to prepare samples for transmission electron microscopy (TEM) the TVM-Cu grids were glued on glass substrates (3–10 mm from its bottom end) and crystals grew directly on the grids. TEM images of HA crystals were recorded using a Zeiss Libra 120 microscope (Carl Zeiss SMT AG Company, Oberkochen, Germany) operated at 120 kV and equipped with a LaB$_6$ emitter with a Koehler illumination

Scheme 1 Hippuric acid, HA (a) and N-(2-thienylcarbonyl)glycine, TG (b).
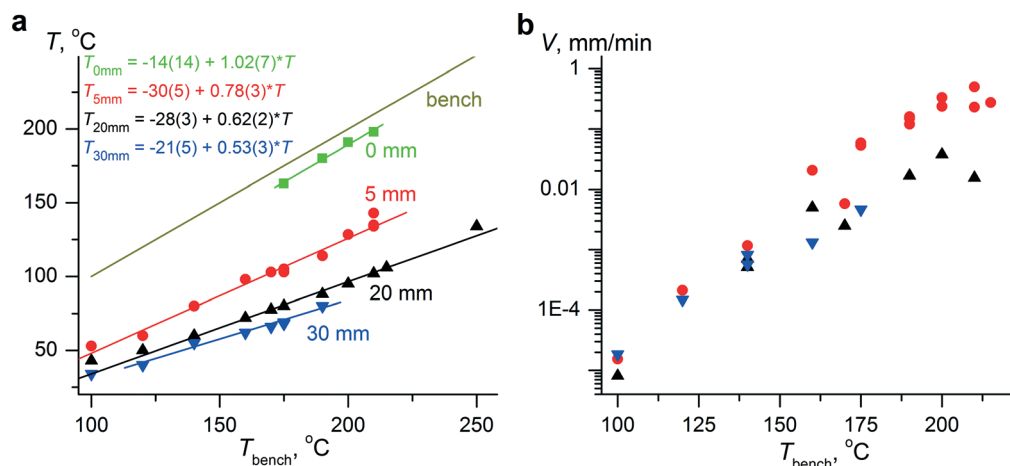
Fig. 2 (a) Temperature (T) at the bottom of a vial (0 mm – green squares) and at different positions on the glass substrate as a function of Kofler bench temperature. (b) Growth rate (V) of HA needles in direction of elongation as a function of Kofler bench temperature (T_{bench}). In both plots red circles, black up-triangles, and blue down-triangles correspond to positions on a glass substrate from the bottom of the vial at 5, 20, and 30 mm, respectively.

system. TEM measurements for TG were performed using a FEI Tecnai 10 electron microscope (FEI Company, Eindhoven, NL) with a LaB$_6$-source at 100 kV acceleration voltage. Images were recorded with a Tietz slow scan CCD F224HD TVIPS camera (pixel size 24 μm, digitization 16 bit) with an active area of 49 mm × 49 mm (Tietz Video and Image Processing Systems GmbH, Gauting, Germany).

Results

The HA and TG crystals grow from the vapor as [100] elongated needles were shaped by the prism {011}, pinacoid {100}, and sometimes minor {101} and {010} faces (Fig. 3a). Twisting was concomitant with a color change of the melts. In this case the crystal tips become elongated or even blade-like with high width (H) to thickness (h) aspect ratios up to 30:1 (Fig. 3b, c, g). Far from the growth front (the growing tip) all four {011} faces grow with similar rates (Fig. 3e). Near the crystal tip (011) and (0$\bar{1}\bar{1}$) faces are no longer the same size as symmetry related (0$\bar{1}$1) and (0$\bar{1}$1) faces. As step growing toward (100) on the diad related (011) and (01$\bar{1}$) faces are inequivalent, the morphology tapers. The symmetry breaking non-equivalence of {011} faces seems to actualize a twist moment at the growth front (Fig. 3c) by reducing h. A typical twisted needle is shown in Fig. 3g, see also Fig. 1b in ref. 1.

AFM images show that the {011} faces grow by steps flowing (Fig. 4) toward the crystal tips. As a result, needles are thicker at the substrate (Fig. 3b, e) or near branching points (Fig. 3d), areas characterized by high dislocation densities that are able to generate steps. The step height was measured to be close to the height of the elementary layer on {011}, $\Delta r = 0.7$ nm.

Crystals can nucleate and grow along the whole substrate length. Most often crystals formed within 5 mm of the bottom of the vial are not twisted whereas crystals formed at 10–20 mm from the bottom are twisted. At the upper part of the

substrate, crystals are infrequent and straight. Twisted crystals formed at the upper part of the substrate only at low temperatures, T_{bench} = 100 °C. We did not find any correlation between twist period and bench temperature, substrate temperature, and, respectively, growth rate in the range T_{bench} = 100–215 °C and $V_{[100]}$ = 10^{-5} – 0.5 mm min^{-1}, respectively (Fig. S2†).

The only variable strongly affecting twist period is crystal cross section. SEM images show that P increases (intensity of twisting, $\theta = \pi/P$, decreases) as the size of a cross section (thickness, h, and width, H) of the needle increases. Since the aspect ratio H/h is not constant an effective crystal radius, r, was calculated assuming the constancy of the torsion constant (rigidity of a cross section against torque) $J = \pi r^4/2 = (0.332H-0.203h)h^3$.[21,22] The plots $P(r)$ for all vapor grown HA and TG crystals show near linear relationships, $n = 1.13$ and $n = 0.83$, respectively (Fig. 1 and 5). Similar relationships were discovered for the melt grown HA crystals[12] and melt and solution grown HA crystals[13] (Fig. 1 and 5).

Bright field TEM images show homogeneous contrast near the tips of several twisted needles and indicate the absence of dislocations in these regions (Fig. 6). Selected area electron diffraction (Fig. 6d) was consistent with a single crystal.

Discussion

The tip is the thinnest part of the crystal (r_0 = 0.05–0.6 μm) and is characterized by the smallest pitch and the sharpest twist (P_0 = 10–380 μm; $\theta_0 = \pi/P_0 \approx$ 0.5–18°/μm). As crystals thicken they begin to untwist. This process was observed *in situ* for the HA needles growing from the melt[12] as well as for melt grown mannitol fibers[23] and solution grown oxalic acid dihydrate[7,24] and gypsum.[25] Post-growth observations presume that many other crystals including quartz have undergone the process of untwisting.[7,26]
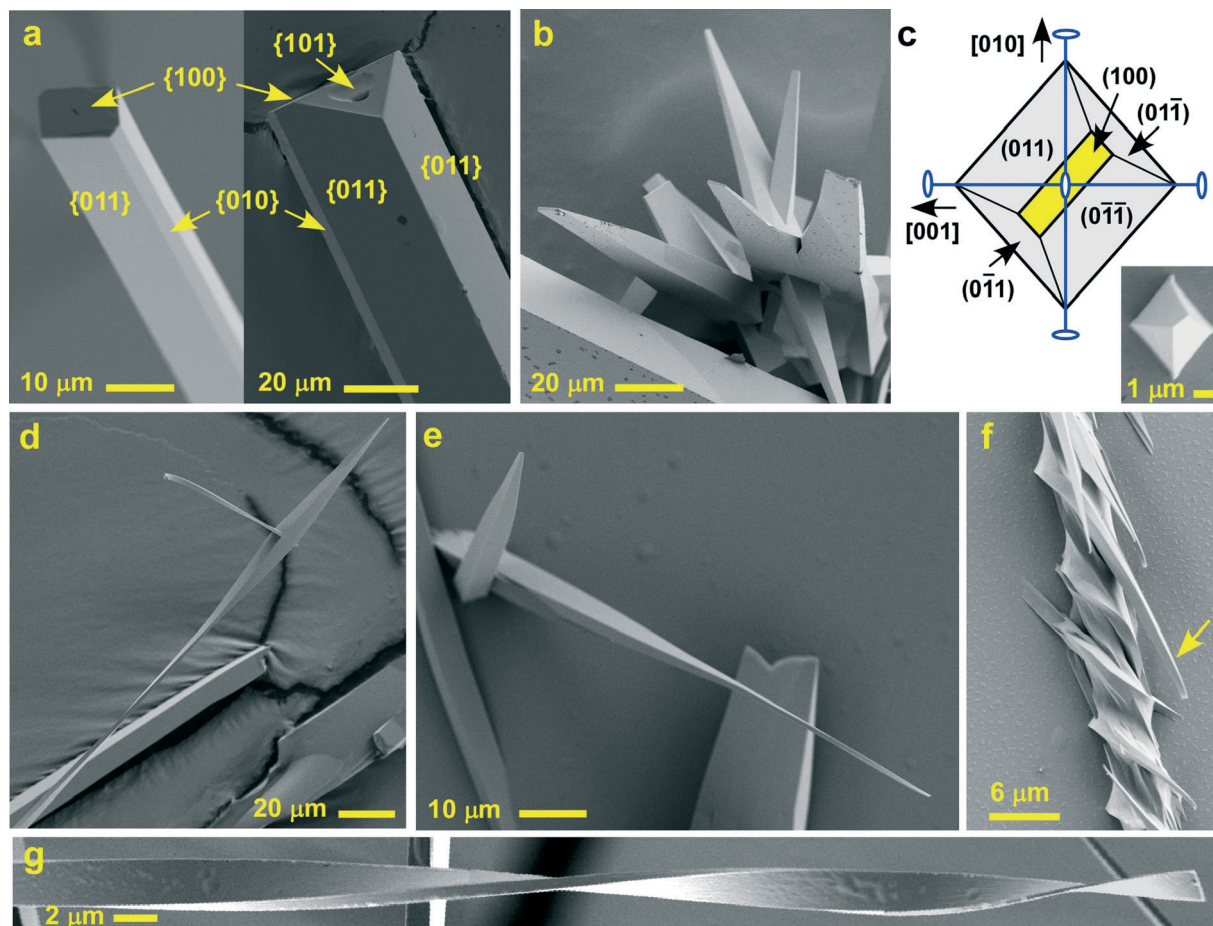
Fig. 3 SEM images showing morphology of HA (a–f) and TG (g) crystals. (a) Straight crystals with indexed growth faces. (b) Tapering of crystal tips. (c) Scheme and micrograph illustrating tapering and loss of morphological crystal symmetry at the growth tip. (d) Thickening of the needle in vicinity of the branching point. (e) Highly anisometric tip thickens and becomes more isometric near the substrate. (f) Needle attached to the substrate surface is strongly twisted whereas a free standing branch of the same crystal indicated by yellow arrow is barely twisted. (g) Typical twisted needle.

Analysis of untwisting dynamics requires knowledge of $P(r)$ for the whole crystal length. Such data were obtained for

ten needles plotted in Fig. 7 as dimensionless P/P_0 *vs.* r/r_0, where the subscript 0 refers to the tip of the crystal. One can
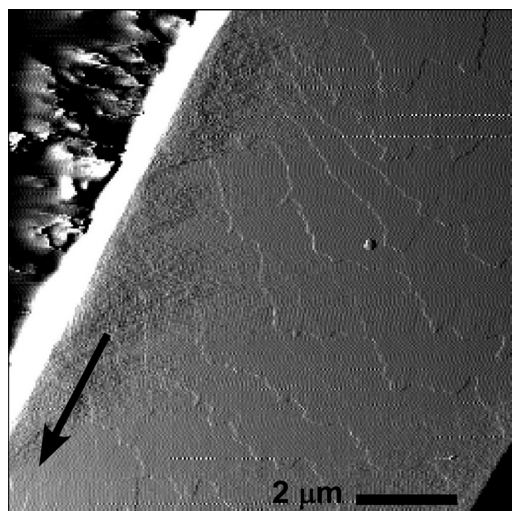

Fig. 4 AFM image of the {011} face of HA crystal. The arrow is pointing toward the crystal tip.
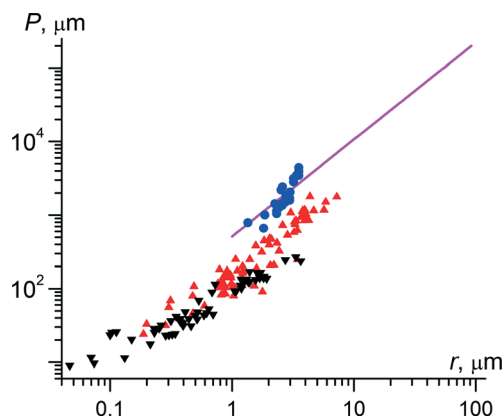

Fig. 5 Consequence of effective cross section radius, r, on twist period, P, of vapor grown HA (red up triangles; $P = 10^{2.17(2)}r^{1.13(6)}$; $N = 118$), vapor grown TG (black down triangles; $P = 10^{1.95(2)}r^{0.83(3)}$; $N = 59$); melt grown HA (blue circles; $P = 10^{2.43(10)}r^{1.94(22)}$; $N = 25$),[12] and solution and melt grown HA (magenta line, $P = 51.1r^{1.32}$; $N = 60$).[13] P and r are given in μm.
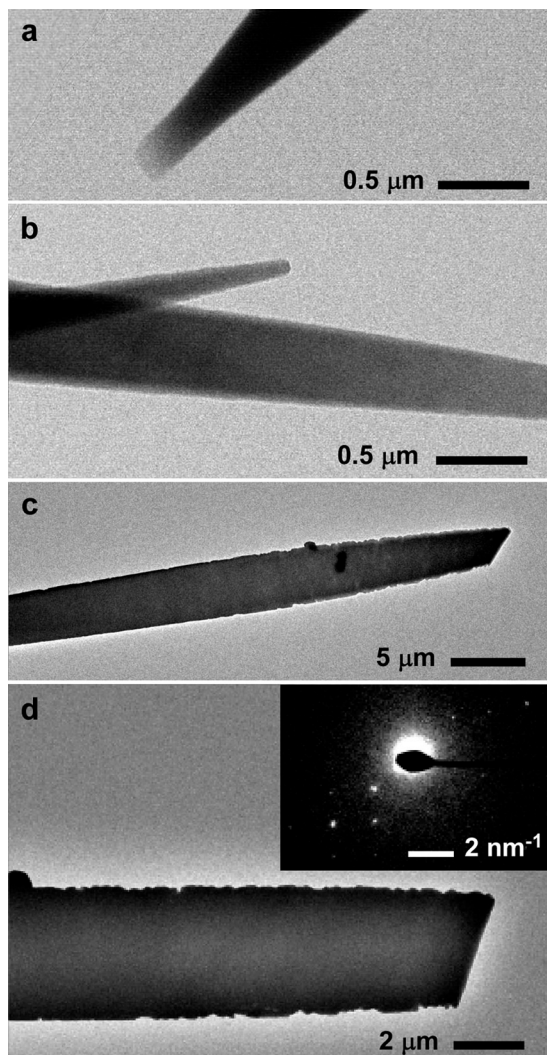
Fig. 6 Bright field TEM images of HA (a, b) and TG (c, d) needles. Image (d) is enlarged image of the crystal shown in (c). Inset shows selected area electron diffraction pattern.

see that P/P_0 increases linearly with r/r_0 for all crystals up to $r/r_0 = 6$. At higher radii only two crystals start showing significant deviations from linearity. Moreover, the slope of P/P_0-(r/r_0) in Fig. 7a falls between 0.4 and 1.5 with most points grouped around 0.6. Keeping these relations in mind, we have built several phenomenological models described below. The models are phenomenological because they analyze the behavior of the system without specifying the actual forces acting on a growing crystal. The following assumptions were used in all models.

1. The crystal shape is assumed to be a cylinder at any given cross section (Fig. 8 and 9). All zones $i = 1,..N$ have a thickness of one elementary growth layer, $\Delta r = 0.7$ nm. The torsion constant for a single layer with internal and external radii r_{i-1} and r_i is given by eqn (1)[22]

$$J_i = \pi(r_i^4 - r_{i-1}^4)/2 \qquad (1)$$

2. Deformation on the boundary between the newly formed layer and the core is consistent. That means that the total (elastic + plastic) strain does not have discontinuities and the total twist intensity $\theta_{T(i)}$ at time (i) is constant over the cylinder cross section

$$\theta_{p,i} + \theta_{e,i} = \theta_{T(N)} = \text{const}, \ \ i = 0,.. N. \qquad (2)$$

Here, subscripts e and p mean elastic and plastic contributions to the twist deformation in zone i, respectively. The subscript (N) next to T denotes time when the Nth zone was growing. It is written in parentheses to distinguish the time step (N) from the growth zone N (Fig. 8).

3. The crystal is in a mechanical equilibrium so that the total twist moment is zero[22]

$$M = \sum_{i=0}^{N} M_i = \sum_{i=0}^{N} G J_i \theta_{e,i} = 0, \qquad (3)$$

where G is the shear modulus.

4. Mechanical twist is manifest in the crystal core corresponding to the subvolume formed by the (100) face (yellow region in Fig. 9a). Stress relaxation relieves the moment accordingly; the moment becomes zero if relaxation is complete. In the latter case, twisting occurs only at the tip of the crystal. The observed total twist intensity at the tip is $\theta_0 = \theta_{p,0} + \theta_{e,\text{tip}} = \theta_{p,0}(1 + \beta) = \pi/P_0$, where $\beta = \theta_{e,\text{tip}}/\theta_{p,0}$ is the ratio between elastic and plastic contributions to the twist at the crystal tip.

5. In the absence of the aforementioned condition, elastic stress relaxes completely at the tip leading to a twisted but stress free crystal core with the intensity of deformation $\theta_{p,0} = \pi/P_0$ and $\beta = 0$ (Fig. 8). A significant degree of stress relaxation is supported by the estimate of the maximum shear strain in the cross section $\gamma = \theta r \approx \pi h/(2P)$ that significantly exceeds the upper limit of yield strain (10^{-3}) in most of materials at high temperatures $T/T_\text{m} > 0.65$ (Fig. 1). During subsequent growth, twisting forces are no longer sufficient and the crystal untwists due to the increased rigidity of the cross section.

Model 1. Plastic stress relaxation is absent providing $\theta_{p,i} = 0$ for all $i = 1,..N$ (Fig. 9b). Solution to eqn (1)–(3) gives

$$\frac{P_N}{P_0} = \frac{\theta_{p,0}}{\theta_{T(N)}} = \left(\frac{r_N}{r_0}\right)^4, \qquad (4)$$

where $P_N = \pi/\theta_{T(N)}$ is a pitch observed at time N. Such a strong twisting dependence on radius has been never observed for any crystal (Fig. 1) including HA and TG (Fig. 7a). This confirms a significant role for plastic relaxation.

Model 2. If there is an axial screw dislocation (Fig. 9e) the stress in the crystal core is not fully elastic near the dislocation whose size is small and comparable with the Burgers vector of the dislocation, b (assumption 5 does not hold). This special case corresponds to Eshelby twisting,[1,2] for which $\theta = b/(\pi r^2)$, and
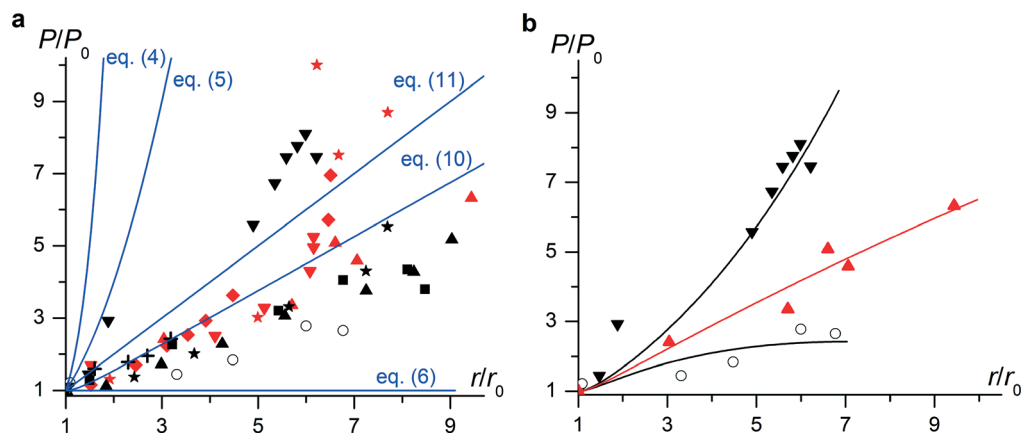
Fig. 7 (a) Dimensionless twist period as a function of cross sectional radius for four HA (red symbols) and six TG (black symbols) needles. Blue lines correspond to five theoretical models linked to the text by the equations specified. (b) Data for one HA and two TG needles from (a) fit with eqn (9). For upper, middle, and lower lines α are equal to 0.9995, 1.000025, and 1.0011 and r_0 are equal to 0.22, 0.60, and 0.11 μm, respectively.
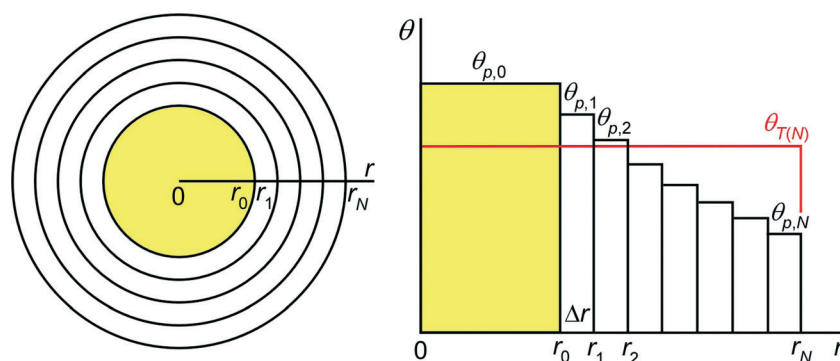

Fig. 8 Schematic showing plastic ($\theta_{p,0}$) and total ($\theta_{T(N)}$) twist intensity along the radius of the thickening rod. Yellow coloration depicts the core growth sector formed by the (100) face.
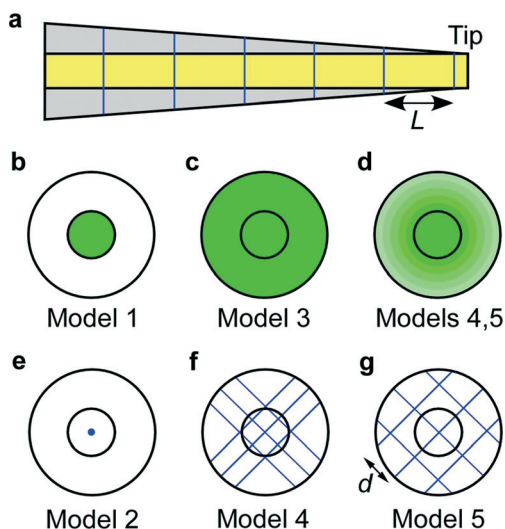

Fig. 9 Schematic representation of HA and TG needles (a) and their cross sections (b–g) for different models of stress relaxation. Yellow and gray areas in figure (a) correspond to parts formed by (100) and {011} faces, respectively. In figures (b)–(e) intensity of green coloration is proportional to the plastic contribution to the twist deformation, θ_p. Blue lines in figures (a), (f), and (g) correspond to screw dislocations in twist boundaries. Blue dot in figure (e) depicts a screw dislocation oriented perpendicular to the cross section of the crystal.

$$\frac{P_N}{P_0} = \left(\frac{r_N}{r_0} \right)^2. \tag{5}$$

Model 3. Formation of new layer is not accompanied by elastic stress or it is accompanied by elastic stress that cannot affect pitch (Fig. 9c). In other words, $\theta_{e,i} = 0 (i = 0,..N)$ and

$$P_N = P_0 \tag{6}$$

Such a situation is realized if a crystalline needle is pinned by the substrate surfaces (Fig. 3f; see also Fig. 23a in ref.1). The pitch of the needle shown in Fig. 3f is equal to $P = 14$ μm. This is close to the lower limit of typical pitches measured at needle tips (P_0 = 10–380 μm). Such tight pitches assume little to no untwisting as the crystal thickens.

Model 4. The plastic relaxation occurs as long as a layer is exposed to the surface. This assumption reflects the fact that relaxation in a surface layer is much faster than in the crystal interior and it is consistent with the assumption that twisting is produced only at the growth tip. The plastic strain in a new layer is assumed to be proportional to the plastic strain

in the underlying layer $\gamma_{p,i} = \gamma_{p,i-1}\alpha$, where α is a parameter. In a twisted cylinder $\gamma = \theta r$. This condition, combined with the relation between strain in adjacent layers, leads to a gradual decrease of $\theta_p(r)$ (Fig. 9d) and results in

$$\theta_{p,i} = \frac{r_{i-1}}{r_i}\theta_{p,i-1}\alpha, i = 1,..N \ . \tag{7}$$

The physical meaning of this expression is that all ($\alpha = 1$) or some fraction ($0 \leq \alpha < 1$) of twist generating defects from the underlying layer penetrate into a new layer. If $\alpha > 1$, defects are multiplied. Substituting eqn (1) and (2) into eqn (3) one can get eqn (8)

$$\left(\theta_{T(N)} - \theta_{p,0}\right)r_0^4 + \sum_{i=1}^{N}\left(r_i^4 - r_{i-1}^4\right)\left(\theta_{T(N)} - \theta_{p,i}\right) = 0, \tag{8}$$

which together with eqn (7) finally provides

$$\frac{P_0}{P_N} = \frac{r_0}{r_N^4}\left(r_0^3 + \sum_{i=1}^{N}\left(r_i^4 - r_{i-1}^4\right)\frac{\alpha^i}{r_i}\right). \tag{9}$$

$P(h)$ is simulated directly using eqn (9) (as well as eqn (12) below) but it is useful to reformulate problem assuming continuous growth – see ESI. If $\alpha = 0$, we get eqn (4) corresponding to model 1. If $\alpha = 1$, neither the defect density in the cross section nor their distribution changes as the crystal thickens. The physical analog of such a model is formation of twist boundaries in the area of the crystal tip with immobile dislocations (Fig. 9f). Twist boundaries are equally spaced along the needle. This leads to significant simplification of eqn (9):

$$\frac{P_N}{P_0} = \frac{3\left(r_N/r_0\right)^4}{4\left(r_N/r_0\right)^3 - 1} \approx \frac{3r_N}{4r_0}, \tag{10}$$

where the approximate equality becomes correct for $r_N > 2r_0$. Eqn (10) agrees well with the experimental data up to $r/r_0 = 6$ (Fig. 7a) suggesting that the simple penetration of all preexisting defects into a new layer is a reasonable assumption. At higher r/r_0 ratios, data deviates from the prediction by eqn (10), suggesting that γ progressively decreases or increases with r. By, slightly varying the parameter α near unity as in eqn (9) whereby a small fraction of defects die or multiply, a better fit is achieved. (Fig. 7b).

Model 5 uses all assumptions of model 4 with one exception: defects are supposed to be mobile and can redistribute as the crystal grows. The overall amount of defects is constant as before. This case corresponds to twist boundaries forming in the area of the crystal tip. However unlike model 4, dislocations are mobile and tend to be equally spaced in the cross section area (Fig. 9g). Formally, $\theta = \pi/P = \omega/L = b/dL$, where ω is the angle of lattice rotation at the twist boundary, L is spacing between neighboring boundaries (Fig. 9a), and d is the distance between dislocations in the array. Since the

number of dislocations, m, is considered to be constant, $d = 2r/m$ and

$$\frac{P_N}{P_0} = \frac{r_N}{r_0}. \tag{11}$$

Eqn (11) describes experimental data reasonably well not as well as eqn (10) (Fig. 7a).

Model 6. It is possible that elastic stress at the growth tip does not relax completely (assumption 5 is not valid). Thus, there is a residual stress that contributes to the twist intensity, $0 < \beta = \theta_{e,tip}/\theta_{p,0} < \infty$. This is similar to model 4. eqn (9) now becomes

$$\frac{P_0}{P_N} = \frac{r_0}{r_N^4}\left(r_0^3 + \frac{1}{1+\beta}\sum_{i=1}^{N}\left(r_i^4 - r_{i-1}^4\right)\frac{\alpha^i}{r_i}\right). \tag{12}$$

If $\beta \to \infty$ (plastic relaxation is absent), eqn (12) reduces to pure elastic deformation (model 1 and eqn (4)) whereas if $\beta = 0$ (relaxation at the tip is complete) we devolve to model 4 and eqn (9). In the case of $\alpha = 1$, eqn (12) is simplified as

$$\frac{P_N}{P_0} = \frac{3(1+\beta)\left(r_N/r_0\right)^4}{4\left(r_N/r_0\right)^3 + 3\beta - 1}. \tag{13}$$

This expression gives similar near-linear $P(r)$ dependence as for eqn (10) but with a larger slope. Most of our experimental data, however, is better fit if stress relaxation at the growth tip is complete, $\beta = 0$.

Thus, experimental data can be reasonably well described with a model for which the driving force for twisting acts at the crystal tip. The elastic stress at the tip undergoes complete plastic relaxation and the density of twist generating defects (plastic shear strain γ_p) remains constant everywhere in the cross section as the crystal thickens. Twist boundaries forming at the crystal tip and evenly distributed along the crystal length can perfectly simulate this mechanical behavior. The dislocation density required to produce the observed twist deformation is known to be $\rho = \theta/b = \pi/(bP)$.[27] Using twist period $P = 0.01–2$ mm (Fig. 5) and $b \approx 1$ nm one can estimate dislocation density on the {011} faces as $\rho \approx 1.5–300$ μm^{-2}. However, TEM (Fig. 6) and AFM (Fig. 4) images show a dislocation density of near zero ($\rho < 0.01–0.1$ μm^{-2}) suggesting that twisting deformation in HA and TG needles is not dislocation mediated.

The minimum lattice mismatch that is required to twist a crystal with radius r can be estimated as $\varepsilon_{min} = \pi r/P$.[12,28] Calculations show that for vapor grown TG and HA crystals (Fig. 5) $\varepsilon_{min} = 0.006–0.06$. Such big lattice mismatch between different regions of the same crystal is very likely a consequence of impurities. Efforts to identify such impurities have thus far been unsuccessful. Moreover, since HA forms twisted crystals from the melt, and the vapor, as well as from

solution, it is unlikely that a phantom decomposition product could shadow HA in all phases of matter.

Conclusions

Excluding the special case of Eshelby twist,[2,3] the majority of twisted crystals shows a linear relationship between twist period and minimal crystal thickness in the cross section, $P = k_0 + k_1 h$. Analysis of vapor grown crystals of HA and TG supports the following mechanism of deformation evolution: Elastic twisting deformations occurring at the crystal tip undergo rapid and complete plastic relaxation. Material precipitating at side faces thickens crystals inducing partial untwisting. The $P(h)$ dependence assumes a constant defect density in each new growth layer. However, microstructural analysis indicates that the defects are not dislocations in the traditional sense.

Acknowledgements

References

1 A. G. Shtukenberg, Y. O. Punin, A. Gujral and B. Kahr, *Angew. Chem., Int. Ed.*, 2014, **53**, 672–699.

2 J. D. Eshelby, *J. Appl. Phys.*, 1953, **24**, 176–179.

3 M. J. Bierman, Y. K. Lau, A. V. Kvit, A. L. Schmitt and S. Jin, *Science*, 2008, **320**, 1060–1063.

4 H. J. Frost and M. F. Ashby, *Deformation-Mechanism Maps: The Plasticity and Creep of Metals and Cera*, Pergamon Press, Oxford, UK, 1982.

5 J. P. Poirier, Creep of Crystals: High Temperature Deformation Processes in Metals, *Ceramics and Minerals*, Cambridge Univ. Press, Cambridge, UK, 1985.

6 G. G. Laemmlein, *Izv. Akad. Nauk SSSR, Ser. Geol.*, 1937, 937–964, published in Russian.

7 Y. O. Punin and A. G. Shtukenberg, *Autodeformation Defects in Crystals*, St. Petersburg Univ. Press, St. Petersburg, Russia, 2008, published in Russian.

8 M. Žorž, *Geologija*, 1994, **36**, 211–222.

9 J. Suda and M. Matsushita, *J. Phys. Soc. Jpn.*, 1995, **64**, 348–351.

10 H. Imai and Y. Oaki, *Angew. Chem., Int. Ed.*, 2004, **43**, 1363–1368.

11 K. Kawabata, T. Kumagai, M. Mizutani and T. Sambongi, *J. Phys. I*, 1996, **6**, 1575–1580.

12 A. G. Shtukenberg, J. Freudenthal and B. Kahr, *J. Am. Chem. Soc.*, 2010, **132**, 9341–9349.

13 P. D. Calvert and D. R. Uhlmann, *J. Polym. Sci., Part B: Polym. Phys.*, 1973, **11**, 457–465.

14 C. Kubel, D. P. Lawrence and D. C. Martin, *Macromolecules*, 2001, **34**, 9053–9058.

15 H. S. Nagaraja, V. Upadhyaya, P. M. Rao, P. S. Aithal and A. P. Bhat, *J. Cryst. Growth*, 1998, **193**, 674–678.

16 D. J. Carter, A. L. Rohl, A. Shtukenberg, S. D. Bian, C. H. Hu, L. Baylon, B. Kahr, H. Mineki, K. Abe, T. Kawasaki and K. Soai, *Cryst. Growth Des.*, 2012, **12**, 2138–2145.

17 F. Bernauer, "*Gedrillte*" *Kristalle*, Gebrüder Borntraeger, Berlin, 1929.

18 N. H. Hartshorne, *Nature*, 1961, **190**, 1191–1192.

19 A. Shtukenberg, E. Gunn, M. Gazzano, J. Freudenthal, E. Camp, R. Sours, E. Rosseeva and B. Kahr, *ChemPhysChem*, 2011, **12**, 1558–1571.

20 A. N. Winchell, *The Optical Properties of Organic Compounds*, McCrone Research Institute, Chicago, 1987.

21 N. M. Beljaev, *Strength of Materials*, Nauka, Moscow, 1965, published in Russian.

22 S. Timoshenko and J. N. Goodier, *Theory of Elasticity*, McGraw Hill, Singapore, 1982.

23 A. G. Shtukenberg, X. Cui, J. Freudenthal, E. Gunn, E. Camp and B. Kahr, *J. Am. Chem. Soc.*, 2012, **134**, 6354–6364.

24 Y. O. Punin and O. M. Boldyreva, *Physics of Crystallization*, Kalinin Univ. Press, Kalinin, 1980, pp. 46–55, published in Russian.

25 Y. O. Punin and O. I. Artamonova, *Crystallogr. Rep.*, 2001, **46**, 138–143.

26 M. A. Kuz'mina, Y. O. Punin and I. E. Kamentsev, *Zap. Vses. Mineral. O-va.*, 1987, **116**, 445–453, published in Russian.

27 N. A. Fleck, G. M. Muller, M. F. Ashby and J. W. Hutchinson, *Acta Metall. Mater.*, 1994, **42**, 475–487.

28 X. Cui, A. L. Rohl, A. Shtukenberg and B. Kahr, *J. Am. Chem. Soc.*, 2013, **135**, 3395–3398.